Eur. Phys. J. D (2017) 71: 127
DOI: 10.1140/epjd/e2017-70713-x

THE EUROPEAN PHYSICAL JOURNAL D

Regular Article

Double ionization of helium by proton impact: from intermediate to high momentum transfer*

Marcelo J. Ambrosio[1,a], Lorenzo U. Ancarani[2], Antonio I. Gómez[3,5], Enzo L. Gaggioli[4,5], Darío M. Mitnik[4,5], and Gustavo Gasaneo[3,5]

[1] Department of Physics, Kansas State University, Manhattan, Kansas 66506, USA
[2] Théorie, Modélisation, Simulation, SRSMC, UMR CNRS 7565, Université de Lorraine, 57078 Metz, France
[3] Departamento de Física, Universidad Nacional del Sur, 8000 Bahía Blanca, Buenos Aires, Argentina
[4] Instituto de Astronomía y Física del Espacio (IAFE, CONICET–UBA), Casilla de Correo 67 – Suc. 28 (C1428ZAA), Ciudad Autnoma de Buenos Aires, Argentina
[5] Consejo Nacional de Investigaciones Científicas y Técnicas, 1430 Buenos Ares, Argentina

Received 15 November 2016 / Received in final form 17 January 2017
Published online 25 May 2017 –

Abstract. We study theoretically the double ionization of helium by 6 MeV proton impact. For such fast projectiles, when considering the projectile-target interaction to first order, the four-body Schrödinger equation reduces to solving a three-body driven equation. We solve it with a generalized Sturmian functions approach and, without evaluating a transition matrix element, we extract the transition amplitude directly from the asymptotic limit of the first order scattering solution. Fivefold differential cross sections (FDCS) are calculated for the double ionization process for a number of coplanar kinematical situations. We present a detailed theory-experiment comparison for intermediate momentum transfers (from 0.8 to 1.2 a.u. and from 1.4 to 2.0 a.u.). In spite of some experimental restrictions (energy and momentum ranges) and the low count rates, we found that our theoretical description provides a very satisfactory reproduction of the measured data on relative scale. We then explore how the binary, recoil and back-to-back structures change with increasing momentum transfers (0.853 to 1.656, to 3.0 a.u.). Within the impulsive regime, with a momentum transfer of 3.0 a.u., we also analyze the FDCS for different excess energies. Finally, in analogy to an experimentalist gathering electrons with different excess energies to obtain enough counts, we provide a *collective* FDCS prediction that hopefully will stimulate further measurements.

1 Introduction

The study of double ionization of simple atoms by charged particle or photon impact allows for a rich investigation of reaction dynamics, and a way to test electron-electron correlation effects. Charged particles, in contrast to photons, can transfer a significant momentum to the target and the dynamics is less understood. In the case of a helium target, doubly ionized by impact of an electron or a proton, we have a pure four-body Coulomb scattering problem which poses a formidable challenge to theoreticians. The most detailed information on the double ionization process is gained from fully, fivefold, differential cross sections (FDCS). Experimentally, however, measuring such a quantity is rather difficult because of low count rates. This is particularly true for protons; as a consequence, compared to the electron impact case, so far only one experiment [1] has provided FDCS, while several measured total cross sections and double-to-single ionization ratios are available (e.g., [2–5]). The 6 MeV differential cross sections measured by Fischer et al. [1] were later integrated to yield doubly differential cross sections [6,7]. The data were further analyzed through so-called four-particle Dalitz plots, and comparisons with other projectiles was made with respect to the projectile charge to speed ratio [8,9].

From a theoretical viewpoint, calculations FDCS for proton-helium double ionization are very scarce [10–12]. A more abundant literature is available, though, for less differential cross sections (see, e.g., [13–17] and references therein). In the present work we present a detailed theoretical study of FDCS for the double ionization of helium by 6 MeV proton impact. In our formulation, the four-body Schrödinger equation corresponding to the proton-helium system is transformed into a set of driven equations containing successive orders in the projectile-target interaction. The first order driven equation is solved with a generalized Sturmian functions (GSF), ab initio,

* Contribution to the Topical Issue: "Many Particle Spectroscopy of Atoms, Molecules, Clusters and Surfaces", edited by A.N. Grum-Grzhimailo, E.V. Gryzlova, Yu.V. Popov, and A.V. Solov'yov.

[a] e-mail: mj_ambrosio@phys.ksu.edu

approach [12,18,19]. The transition amplitude, extracted from the asymptotic limit of the first order solution, is equivalent to the familiar first Born approximation.

In a previous contribution [12], we focused mostly on a comparison between our ab initio methodology and two different improvements on the 3C model by López et al. [10,11]. All these discussions considered protonic projectiles with an incident energy of 700 keV, implying a velocity of 5.29 a.u. The final part of that manuscript contained a comparison with experimental FDCS [1], having faster projectiles: 6 MeV (velocity: 15.5 a.u.), a regime better suited for our first order Born scheme treatment of the projectile-target interaction. Because the counting rates were so small, the experimentalists had to assemble cross sections containing a range of momentum transfers (direction and magnitude) and energies; as such, the cross sections are not fully differential. From the intermediate momentum transfer results reported in [1], however, we made a successful comparison with those whose kinematic conditions had the narrowest angular range for the momentum transfer vector. The first new results of the present manuscript will show that the agreement was even better than observed in that article. Then we will show a theoretical-experimental comparison for another data series from the same experiment, still at intermediate momentum transfers. Keeping the same incident energy, we then turn our attention to the impulsive regime, i.e., with a high momentum transfer $q = 3$ a.u., and present FDCS for three emission energies. Since it is expected that a further experiment would observe small count numbers, we produce a theoretical FDCS consisting on the addition of the three, analogous to the experimental approach adopted by Fischer et al. [1]. This can be of use should the experimentalists not register enough counts for a more completely differential cross section.

For protonic projectiles at 6 MeV, the experimental cross sections in reference [1] possess the appropriate symmetry to suggest that a first Born order treatment is sufficient to describe the essential physics involved; this was indeed confirmed in our previous study [12]. It should be noted, however, that the situation is quite different for the electron impact case, for which second order effects have been reported even for projectiles with energy as high as 2 keV (see [1,20,21] and references therein). An analysis with respect to the charge and the velocity of the projectile was presented in [1]. While some contributing ionization mechanisms are proportional to even power of the corresponding Sommerfeld parameter, interference between amplitudes do depend on the sign of the projectile. Only a second Born treatment would be able to properly take into account all relevant mechanism; this, however, goes beyond the scope of the present contribution.

The rest of the paper is arranged as follows. In Section 2 we briefly outline the theoretical framework, and the GSF approach to solve the three-body driven equation. Results are presented in Section 3. Finally, a brief summary is provided in Section 4. Atomic units ($\hbar = e = m_e = 1$) are used throughout the article, unless otherwise stated.

2 Fast projectile formulation and GSF approach

The proton-helium collision is a four-body scattering problem. For fast projectiles, one may use a first order treatment in the perturbative series of the projectile-target interaction. The resulting three-body problem takes the form of a driven equation. Here, we solve it with the GSF method.

Let $\mathbf{r}_1$ denote the position of the projectile (mass m_P) and $\mathbf{r}_i$ $(i = 2, 3)$ that of the two helium electrons with respect to its nucleus (mass m_T, charge $Z = 2$), and $r_{ij} = |\mathbf{r_i} - \mathbf{r_j}|$ the distance between particles i and j. The full four-body Hamiltonian reads [11]

$$H = -\frac{1}{2\mu_{TP}}\nabla_1^2 - \frac{1}{2\mu_T}\nabla_2^2 - \frac{1}{2\mu_T}\nabla_3^2 + \frac{Z}{r_1} - \frac{1}{r_{12}} - \frac{1}{r_{13}} - \frac{Z}{r_2} - \frac{Z}{r_3} + \frac{1}{r_{23}}, \quad (1)$$

where the reduced masses $\mu_{TP} = \frac{m_P m_T}{m_P + m_T}$ and $\mu_T = \frac{m_T}{m_T+1}$. Similarly to references [12,18,19], we propose to write

$$H = H_0 + \bar{W}, \quad (2)$$

where

$$H_0 = h_p + h_{\mathrm{He}}, \quad (3)$$

with

$$h_{\mathrm{He}} = \left(-\frac{1}{2\mu_T}\nabla_2^2 - \frac{1}{2\mu_T}\nabla_3^2 - \frac{Z}{r_2} - \frac{Z}{r_3} + \frac{1}{r_{23}}\right) \quad (4)$$

the three-body helium Hamiltonian acting the subsystem (2, 3) and $h_p = -\frac{1}{2\mu_{TP}}\nabla_1^2$ the free-particle kinetic term associated to the projectile 1. The perturbation

$$\bar{W} = \frac{Z}{r_1} - \frac{1}{r_{12}} - \frac{1}{r_{13}} \quad (5)$$

couples the two Hamiltonians h_{He} and h_P.

With such a decomposition, for a total energy E, the four-body Schrödinger equation with outgoing (+) type-behavior reads

$$\left[H_0 + \bar{W} - E\right]\Psi^+(\mathbf{r}_1, \mathbf{r}_2, \mathbf{r}_3) = 0. \quad (6)$$

It can be transformed into a set of coupled driven equations containing successive orders in the projectile-target interaction, as shown in reference [18]. The solution is proposed as:

$$\Psi^+(\mathbf{r}_1, \mathbf{r}_2, \mathbf{r}_3) = \sum_n \Psi^{(n)+}(\mathbf{r}_1, \mathbf{r}_2, \mathbf{r}_3), \quad (7)$$

where each order retains n interactions $\bar{W}$ between the projectile and the target.

The zeroth order equation

$$\left[H_0 - E\right]\Psi^{(0)+}(\mathbf{r}_1, \mathbf{r}_2, \mathbf{r}_3) = 0, \quad (8)$$

corresponds to a separable solution, $e^{i\mathbf{k}_i\cdot\mathbf{r}_1}\ \Phi_i(\mathbf{r}_2, \mathbf{r}_3)$, where $\Phi_i(\mathbf{r}_2, \mathbf{r}_3)$ is the helium ground state and a plane

wave of momentum $\mathbf{k}_i$ describes the fast incident projectile.

Allowing for one interaction only, one needs to solve the first order equation

$$[H_0 - E]\,\Psi^{(1)+}(\mathbf{r}_1,\mathbf{r}_2,\mathbf{r}_3) = -\bar{W}\Psi^{(0)+}(\mathbf{r}_1,\mathbf{r}_2,\mathbf{r}_3)\,. \quad (9)$$

As proposed in [18], the first order solution is written as:

$$\Psi^{(1)+}(\mathbf{r}_1,\mathbf{r}_2,\mathbf{r}_3) = \frac{1}{(2\pi)^{3/2}}\int d\mathbf{k}\; e^{i\mathbf{k}\cdot\mathbf{r}_1}\Phi^{+}_{sc}(\mathbf{k},\mathbf{r}_2,\mathbf{r}_3)\,, \quad (10)$$

where the three-body scattering (label sc) function Φ^{+}_{sc} characterizes the physics of the ejected electrons. Let E_a denote the energy of two electrons in interaction with the nucleus in the final state, and $k^2/2$ the energy associated to the projectile: the total energy of the system is then $E = E_a + k^2/(2\mu_{TP})$. The momentum transfer vector is defined as $\mathbf{q} = \mathbf{k}_i - \mathbf{k}_f$ where $\mathbf{k}_i$ is the incident and $\mathbf{k}_f$ the scattered momentum.

Replacing equation (10) into (9), one arrives to a driven equation for $\Phi^{+}_{sc}(\mathbf{q},\mathbf{r}_2,\mathbf{r}_3)$ [18]:

$$[h_{\mathrm{He}} - E_a]\,\Phi^{+}_{sc}(\mathbf{q},\mathbf{r}_2,\mathbf{r}_3) = -\frac{4\pi}{q^2}\frac{1}{(2\pi)^3}\left(Z - e^{i\mathbf{q}\cdot\mathbf{r}_2} - e^{i\mathbf{q}\cdot\mathbf{r}_3}\right)\Phi_i(\mathbf{r}_2,\mathbf{r}_3)\,, \quad (11)$$

where the momentum transfer $\mathbf{q}$ dependence is explicit in the three-body scattering wave function.

Formally [22], for large hyperradii $\rho = \sqrt{r_2^2 + r_3^2}$, the asymptotic behavior of $\Phi^{+}_{sc}(\mathbf{q},\mathbf{r}_2,\mathbf{r}_3)$ is directly related to the transition amplitude $T_{\tilde{\mathbf{k}}_2,\tilde{\mathbf{k}}_3}$ through

$$|\Phi^{+}_{sc}(\mathbf{q},\mathbf{r}_2,\mathbf{r}_3)|^2 \underset{\rho\to\infty}{\longrightarrow} (2\pi)\kappa^3|T_{\tilde{\mathbf{k}}_2,\tilde{\mathbf{k}}_3}|^2\frac{1}{\rho^5}, \quad (12)$$

where $\kappa = \sqrt{2E_a}$ is the hypermomentum. In our driven equation approach, therefore, the transition amplitude is extracted from the scattering solution in the double continuum channel. [Note that this approach is equivalent to the more familiar expression used in the FBA, whereby a transition matrix element is calculated; it involves a six dimensional integral corresponding to the projection of the driven term of equation (11) onto the final two-electrons double continuum.]

For two electrons escaping with energies E_2 and E_3 in the solid angles $d\Omega_2$ and $d\Omega_3$, the FDCS – within the FBA – is defined as

$$\frac{d^5\sigma}{d\Omega_2 d\Omega_3 d\Omega_f dE_2 dE_3} = (2\pi)^4\frac{k_f k_2 k_3}{k_i}|T_{\tilde{\mathbf{k}}_2,\tilde{\mathbf{k}}_3}|^2, \quad (13)$$

where the projectile, whose energy $E_f = k_f^2/(2\mu_{TP})$ is determined by total energy conservation, is scattered in the solid angle $d\Omega_f$.

To solve the first order three-body driven equation (11) for a given $\mathbf{q}$ we use a Sturmian approach with one-particle GSF. Details of the method are described in [12,19,23], and will only be briefly outlined here.

For convenience [19,23], the helium ground state is also constructed within the GSF formalism. Negative energies GSF basis can be used efficiently to obtain two-electron bound states [24–27]. Here, like in [12], the helium ground state with an energy of –2.9035 a.u. is obtained with the GSF method [26,27], using 20 Sturmians per coordinate per partial wave, with individual angular momenta up to 4.

In order to calculate the scattering function, we proceed as explained in reference [19]: $\Phi^{+}_{sc}(\mathbf{q},\mathbf{r}_2,\mathbf{r}_3)$ is decomposed in total-angular-momentum partial waves, and subsequently expanded on products of radial GSF with outgoing Coulomb behavior (see Eq. (19) of [19]). This proposal converts the driven equation (11) into a linear system (similar to Eq. (21) of [19]) which is solved with standard methods. In all kinematical configurations considered below, convergence in the number of partial waves has been verified.

Once $\Phi^{+}_{sc}(\mathbf{q},\mathbf{r}_2,\mathbf{r}_3)$ is obtained, we extract from equation (12) the quantity $|T_{\tilde{\mathbf{k}}_2,\tilde{\mathbf{k}}_3}|^2$ at a given large enough ρ value. Finally the FDCS is calculated with expression (13).

3 Results

In this contribution, only coplanar configurations are considered, and all angles are defined with respect to the incident-beam direction. We consider excess energies $E_a = E_2 + E_3$ of 10, 20 and 40 eV, and an equal energy sharing between the ejected electrons 2 and 3, i.e. $E_2 = E_3$. All our calculations include total angular momenta up to 3, while the partial waves contain individual angular momenta l_2, l_3 up to 5. For 5 + 5 eV kinematics we employed a spatial box of 50 × 50 a.u. (ρ = 50 a.u.), while 45 × 45 a.u. for 10 + 10 eV (ρ = 45 a.u.) and 30 × 30 a.u. for 20 + 20 eV (ρ = 30 a.u.) excess energies, using 55, 50 and 40 Sturmian per coordinate per partial wave, respectively. Boxes of similar sizes have been used successfully to compare with other theoretical as well as with experimental cross sections for double ionization of helium by photon [28], electron [19] and proton [12] impact. To properly reach the asymptotic regime, in particular for low excess energies, one could consider larger hyperradii; we have observed, however, that once convergence is reached, the size of the spatial domain only affects the magnitudes and not the FDCS shape (we recall that in the present study we compare with relative experimental data).

We divide our results into two main sections.

– In the first one, we continue the line started in [12], analyzing to a more extensive detail the FDCS that was already shown to agree with the relative scale experiments [1] at intermediate momentum transfer (q in the range 1.4 to 2 a.u.). We delve deeper into the comparison, plotting FDCS for fixed values of θ_2. This type of comparison is locally more stringent than matching the overall experimental and theoretical FDCS shape in terms of both emission angles (contour plots). We then compare fixed-angle FDCS with another experimental data set [29], with a slightly lower momentum transfer in the range 0.8 and 1.2 a.u.

– The second section is dedicated to a theoretical study of the FDCS for an impulsive ($q = 3.0$ a.u.) regime, again under equal energy sharing geometries. For comparison we begin with a fixed excess energy, studying how the FDCS evolves from intermediate momentum transfers to the impulsive regime. Then, within the impulsive regime we present cross sections for different outgoing energies. Considering that experimentalists may have to collect ejected electrons having different excess energies due to low counting rates, we construct also a collective FDCS for electrons emerging with 5 + 5 eV, 10 + 10 eV and 20 + 20 eV.

3.1 Detailed comparison with experimental results at intermediate momentum transfers

We begin by comparing our theoretical FDCS with the relative scale experimental data of Fischer et al. [1]. Due to the low counting rate, the measurements were made with the collection of electrons with $E_2 = E_3 < 25$ eV and momentum transfers ranging in magnitude q from 1.4 to 2.0 a.u. and in angle θ_q from 75° to 85°. As such, the measured cross sections cannot be considered as properly fully differential.

In order to make a theory-experiment comparison, we made a calculation [12] at the intermediate value $\theta_q = 81.85°$ and the total emission energy chosen in the middle of the measured range, i.e., 10 eV per electron. As the experimental momentum transfer ranged from $q_{min} = 1.4$ a.u. to $q_{max} = 2.0$ a.u., we took an averaged value $\langle q \rangle = 1.656$ a.u. obtained through

$$\langle q \rangle = \left[\frac{1}{q_{max} - q_{min}} \int_{q_{min}}^{q_{max}} \frac{1}{q^4} dq \right]^{-1/4} . \qquad (14)$$

The weight in this momentum transfer average is inspired by the fact that the FDCS inherits a factor $1/q^4$ from the transition matrix (see Eqs. (11) and (13)). It will be shown in Section 3.2 that contributions to the electron yield are visibly stronger for smaller momenta transfers, backing the weighted average approach.

Figure 1 shows, as a function of both emission angles, the experimental data, together with our theoretically calculated contour plots (both on relative scales). Similarly to the recent analysis [12,21] of double ionization processes, for compactness and ease of description, we will designate hereafter the binary peak as A, the recoil peak as B and the back-to-back structure as C. The binary peak emerges as the result of one target electron initially absorbing momentum from the projectile, and then colliding with the remaining target electron. The sum of their momenta, $\mathbf{k}_2+\mathbf{k}_3$, points into the direction of $\mathbf{q}$. On the other hand, the recoil peak requires the electron hit by the projectile to perform a recoil off the nucleus, and strike the other electron afterwards, resulting in a momentum sum $\mathbf{k}_2+\mathbf{k}_3$ antiparallel to $\mathbf{q}$. The back-to-back structure, as its name suggests, consists on an emission with both ejected electrons emerging in opposite directions. A classical picture to produce such an emission is as follows: one target

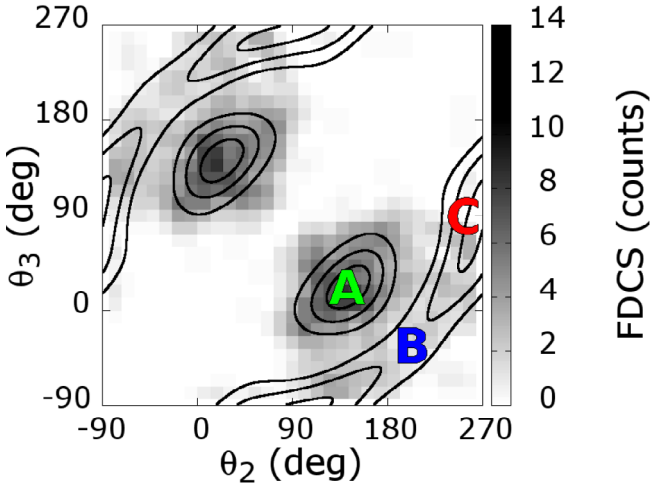

Fig. 1. Theoretical [12] and experimental [1] FDCS overlapped. The binary, recoil, and back-to-back structures are labelled by, respectively, A, B and C.

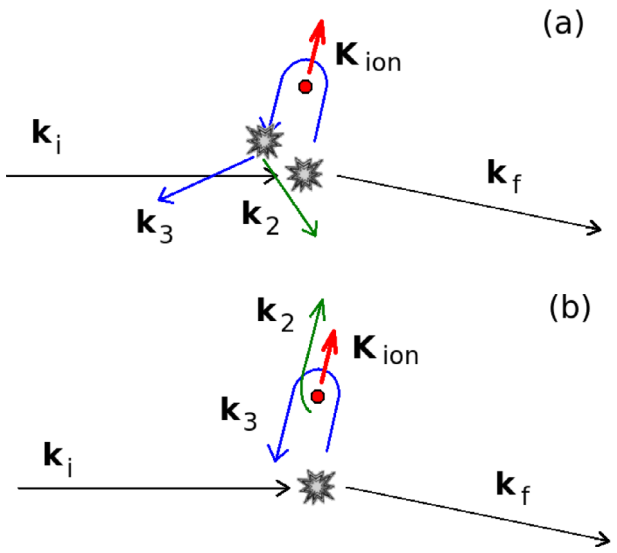

Fig. 2. Schematic representation of the (a) recoil and (b) back-to-back type processes.

electron receives momentum from the projectile, and recoils off the nucleus emerging in a direction antiparallel to $\mathbf{q}$ and giving the nucleus a momentum $\approx -2\mathbf{q}$; the nucleus then scatters the second electron in the $\mathbf{q}$ direction [30]. Figure 2 provides a schematic representation of the recoil and back-to-back processes, which will be discussed later in the text.

Despite the limited amount of counts, the cross section shapes in Figure 1 (theory from Ref. [12], experiment from Ref. [1]) show good agreement. In brief, both have their binary peaks (A) centered at the same angles (θ_2, θ_3). A dip is present in both theory and experiment where the recoil peak (B) would be present for smaller momentum transfers, and this structure is merged with the back-to-back one (C).

A more detailed comparison can be achieved by looking at different fixed θ_2 cuts from the FDCS presented

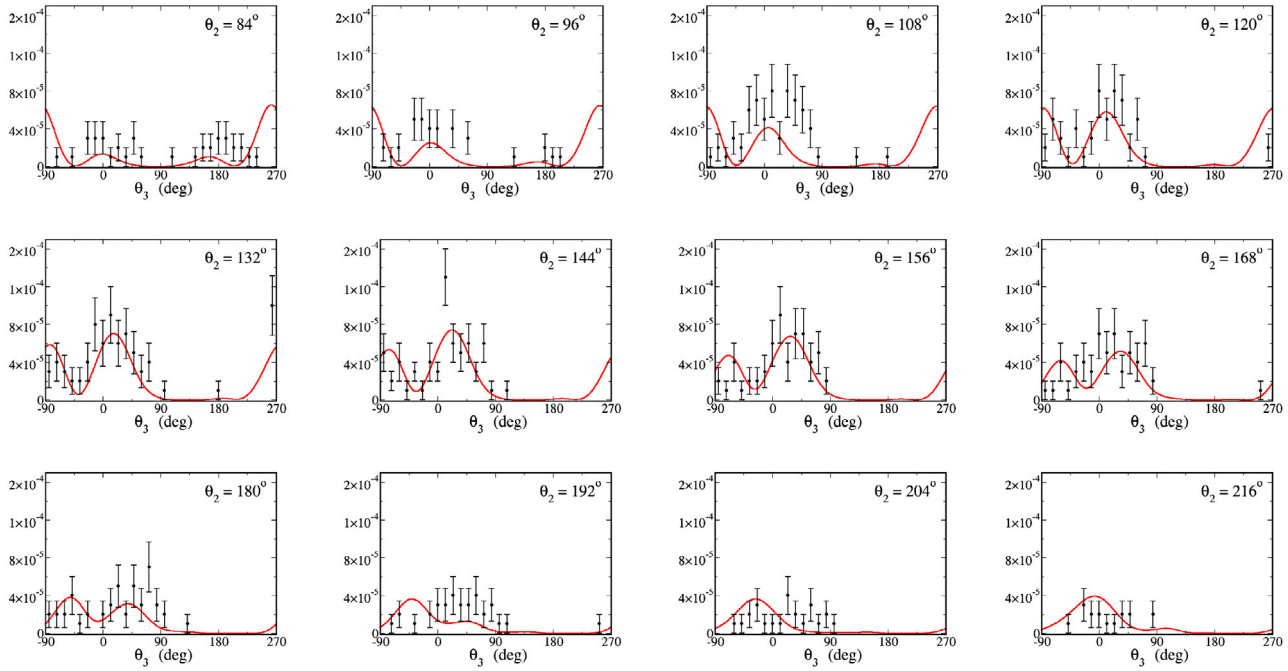

Fig. 3. FDCS in a.u. for fixed indicated θ_2, all with same vertical range. The experimental data correspond to a momentum transfer between 1.4 and 2.0 a.u. [1], while for the theory we used the weighted average $\langle q \rangle = 1.656$ a.u. and the two emitted electrons each take 10 eV [12]. Experimental counts were normalized at the largest peak value to the calculation [12] in order to have the best overall agreement for the $\theta_2 = 156°$ cut.

in Figure 1. They are plotted in Figure 3, where the experimental data was globally normalized to match the tallest structure, A, with our cross section. The observed agreement is even stronger than evidenced by the previous figure. This is quite remarkable if one recalls that our calculation is made with an averaged q value and that experimental data are not proper FDCS. The experimental shapes and height ratios of the structures are rather well reproduced by our theoretical calculations. There are some appreciable departures from the dipolar limit [31]: the recoil (B) and binary (A) peaks are markedly different in shape, and an important back-to-back (C) emission structure is observed.

We continue the analysis, with another set of experimental data provided by Fischer [29], with a momentum transfer ranging from 0.8 to 1.2 a.u., directed at ≈75°. The measurements include the collection of equal-energy-sharing electrons with energies ranging from 10 to 20 eV each. In our calculation, on the other hand, we took the weighted-average momentum transfer (14) $\langle q \rangle = 0.853$ a.u., electrons ejected at 10 + 10 eV, and $\theta_q = 74.09°$. Figure 4 shows a good agreement in the overall placement and shape of the cross section structures. This is again very satisfactory in view of the non-fully differential character of the experimental data. To investigate the issue of the ejected electrons' energy range, we have also calculated, for the same momentum transfer, the 20 + 20 eV kinematical situation (with $\theta_q = 70.76°$). We observed a FDCS roughly four times smaller in magnitude, with a very similar shape. Therefore, the addition of both cross sections is strongly dominated by the 10 + 10 eV one,

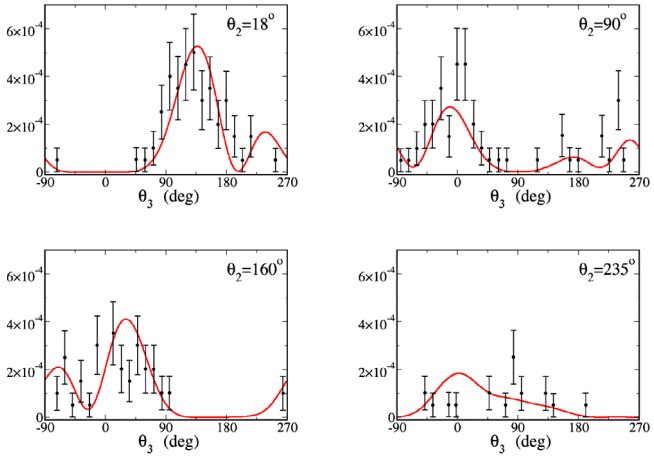

Fig. 4. FDCS in a.u. for fixed indicated θ_2, all with same vertical range. The experimental data correspond to a momentum transfer between 0.8 and 1.2 a.u., while for the theory we used the weighted average $\langle q \rangle = 0.853$ a.u. and the two emitted electrons emerge with kinetic energies of 10 eV. Experimental counts globally normalized to the present theoretical to produce the best overall agreement for the $\theta_2 = 18°$ cut.

and the 20 + 20 eV contribution would essentially add a 25% in magnitude, leaving the TDCS shape essentially unchanged. This means that the experimental-theoretical comparison of Figure 4 remains qualitative; for a quantitative comparison, experiments would need to have narrower excess energy limits.

Table 1. Binary (A), recoil (B) and back-to-back (C) peak heights and peak height ratios, for excess energies of $E_a = (10 + 10)$ eV and for the different momentum transfer values in a.u.

q	A	B	C	B/A	C/A
0.853	6.0E-04	2.0E-04	1.5E-04	0.33	0.25
1.656	2.0E-04	4.0E-05	7.0E-05	0.20	0.375
3.000	2.5E-05	4E-06	2.0E-05	0.16	0.80

In the two momentum transfer intervals analyzed above, the theory-experiment agreement evidences that for proton-helium collisions the first order Born approximation is enough to characterize the dynamics. This is notoriously different for electron impact ionization, where second order effects are strongly evident in experimental cross sections [1,20,21,32,33].

3.2 Theoretical FDCS for the impulsive regime

We turn to explore theoretically the impulsive regime, choosing a momentum transfer $q = 3$ a.u. directed at $\theta_q \approx 85°$. By fixing the excess energy at $E_a = (10 + 10)$ eV, we start by looking at the FDCS evolution as the momentum transfer increases.

Figure 5 shows contour plots of the FDCS for the two cases described in the above section, i.e., $q = 0.853$ and $q = 1.656$ a.u., together with the impulsive regime $q = 3$ a.u. configuration. As the momentum transfer increases (top to bottom) a clear trend towards a more dominant back-to-back emission emerges: it gains in relative magnitude and simultaneously extends to substantially larger angular domains. We also clearly observe that the recoil structure is smeared out.

Quantitatively, all peaks decrease in magnitude as q increases (see Tab. 1). In particular, when the momentum transfer grows from $q = 1.656$ to $q = 3.0$, the binary (A) magnitude experiences a sharp drop that can be understood as follows: as q increases, the time spent by the impacted electron in the area of the nucleus is smaller, reducing the likeliness of a subsequent collision with the other electron. This reasoning also applies for the recoil peak, after the impacted electron recoils off the nucleus. This leads to a recoil-to-binary-peak ratio B/A that is only moderately changed (0.20 to 0.16), considering that the momentum transfer is roughly doubled. On the other hand, back-to-back emission depends weakly on the interelectronic repulsion and only requires electron-nucleus hard interactions: thus the back-to-back (C) magnitude decreases, but to a lesser extent. As a consequence, the peak height ratio C/A increases with q indicating clearly that back-to-back emission gains in relative preponderance.

To gain further insight, we also calculated FDCS under the impulsive regime ($q = 3$) and three equal energy sharing situations: $E_2 = E_3 = 5$ eV, $E_2 = E_3 = 10$ eV and $E_2 = E_3 = 20$ eV. Results are shown in Figure 6. The three evidence the common A, B and C peaks, although with varying relative weights. For the (20 + 20) eV

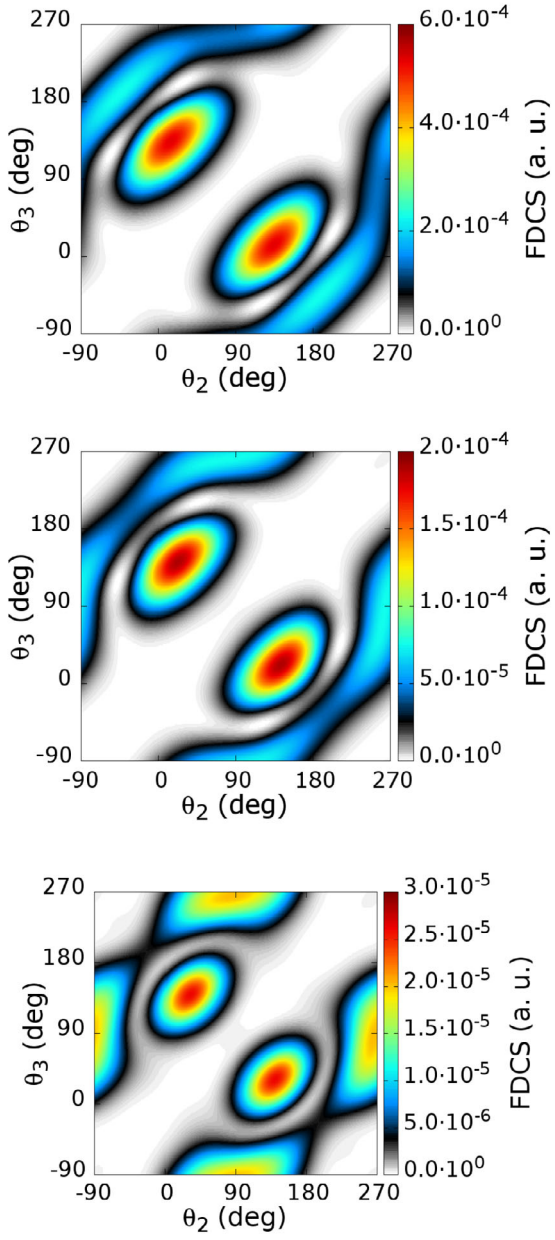

Fig. 5. FDCS in a.u. (intensity scale indicated on the right-hand side) in terms of both emission angles for an excess energy of 10 + 10 eV and for the following momentum transfers: (top) $q = 0.853$ a.u., (middle) $q = 1.656$ a.u. and (bottom) $q = 3.0$ a.u.

excess energy configuration, the high ejection velocities make off-nucleus recoil less probable, and the binary structure dominates the FDCS (see Fig. 6c); the nucleus is a mere spectator. For electrons emerging with (5 + 5) eV (i.e., $k_2 = k_3 = 0.606$ a.u.), on the other hand, the nucleus has to absorb a significant amount of momentum regardless of the emission directions. This allows for more interactions, such as a binary collision followed by one of the electrons performing a subsequent recoil. This scenario [$(\theta_2 \approx 0°, \theta_3 \approx 250°)$ and $(\theta_2 \approx 150°, \theta_3 \approx -70°)$] is compatible with the FDCS in Figure 6a. Emission

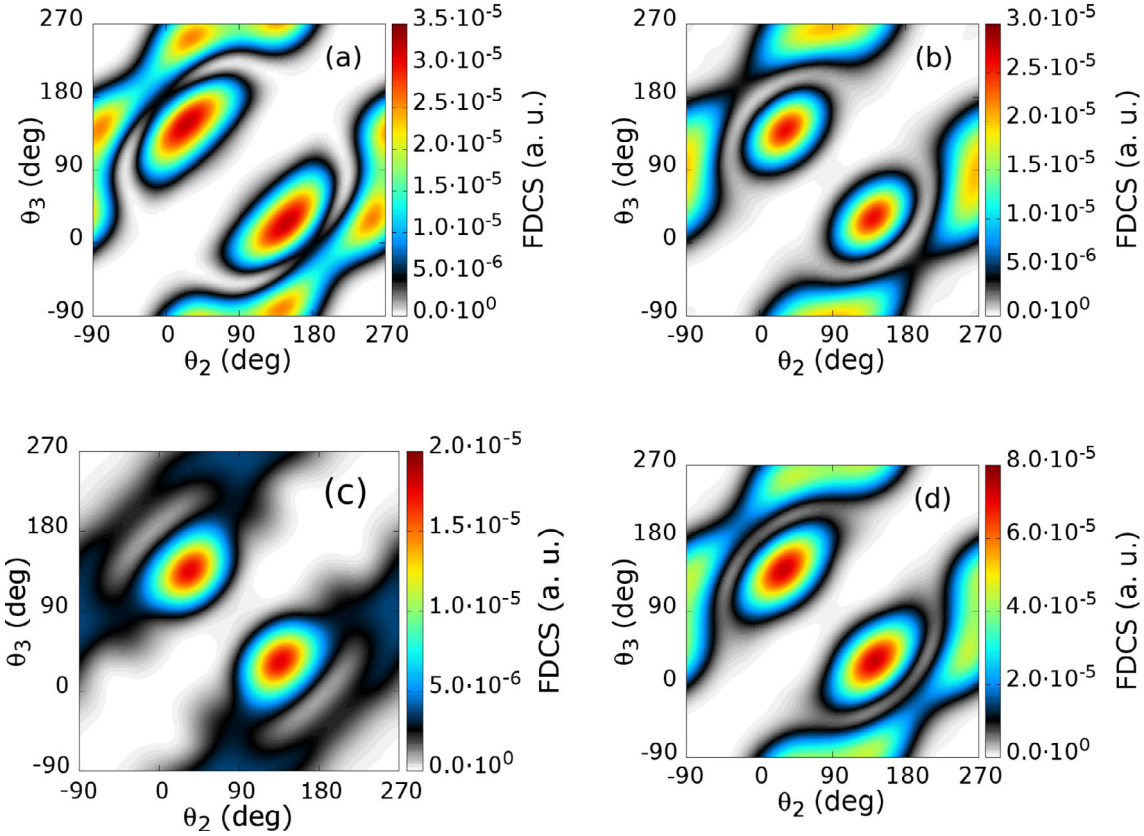

Fig. 6. FDCS in a.u. (intensity scale indicated on the right-hand side) in terms of both emission angles for different excess energies, with a fixed momentum transfer $q = 3$. Excess energies: (a) 5 + 5 eV, (b) 10 + 10 eV, (c) 20 + 20 eV and (d) sum of the three others.

in those directions can also be achieved through a back-to-back process. In ab initio methodologies (like the GSF) it is difficult to separate out, when they can produce equivalent kinematics, the FDCS contribution of each mechanism. Indeed, the scattering wave function $\Psi^{+}_{sc}(\mathbf{q}, \mathbf{r}_2, \mathbf{r}_3)$, obtained in a *numerically exact* fashion, contains simultaneously all physically possible intra-target collision mechanisms.

Since for the impulsive regime the calculated FDCS absolute scale are rather small compared to those presented for lower momentum transfers, we expect that measurements will be rather difficult to perform. Experimentalist may be forced to collect electrons for different excess energies as done by Fischer et al. [1]. In the same spirit, we may increase the number of theoretical counts by summing FDCS contributions corresponding to different final energies; this comes at the cost of losing detailed information about the underlying collision mechanisms. Since the fragments' momenta are well defined both in experiments and in theory, there should be no coherent superposition leading to cross section interference. The incoherent FDCS sum of the three final energy contributions is shown in Figure 6d. The resulting cross section exhibits B and C peaks that blend the contributions from 5 + 5 eV and 10 + 10 configurations, whereas for the A peak there are also relevant contributions from the 20 + 20 eV case. An experiment with equal-energy-sharing electrons from 5 + 5 eV up to 20 + 20 eV would be expected to present a FDCS like the one shown in Figure 6d.

4 Summary

In this contribution we calculated FDCS for proton-impact helium double ionization. For fast projectiles, the four-body problem is reduced to a three-body one (equivalent to a first order Born approach). We used the GSF approach to solve the corresponding driven equation. From the asymptotic double continuum part of the numerical solution, we extracted the transition amplitude and thus the FDCS.

We performed stringent theory-experiment FDCS comparisons, achieving a great degree of accord for intermediate momentum transfer values. Our first order Born treatment for the projectile-target interaction is enough to produce a very good agreement in coplanar geometry, strongly suggesting that it is enough to capture the essence of the collision dynamics involved for protonic projectiles. Keeping the excess energy fixed, we first studied how the FDCS changes with increasing momentum transfers. The shape and relative magnitude variations of the back-to-back and recoil peak are understood in terms of electron-electron and electron-nucleus (recoil) collisions. We then proceeded to analyze the impulsive regime (i.e., a high momentum transfer, $q = 3$ a.u., to the target subsystem),

and described the structures that appear in the FDCS for different excess energies. We finished by offering a collective FDCS for electrons with kinetic energies of 5 + 5 eV, 10 + 10 eV and 20 + 20 eV, in what can be considered as the theoretical counterpart of the experimental procedure followed by Fischer et al. [1] due to the very low counting rates. Our result could be compared with an experiment gathering equal energy electrons with energies ranging from 5 + 5 eV up to 20 + 20 eV for momentum transfers near 3.0 a.u.

We thank Prof. D. Fischer for providing the results of his previous publication in tabular form, as well as the unpublished set. We acknowledge the support by PIP 201301/607 CONICET (Argentina), and one of the authors (G. Gasaneo) also thanks the support by PGI (24/F059) of the Universidad Nacional del Sur. We acknowledge the CNRS (PICS project No. 06304) and CONICET (project No. Dl 158114) for funding our French-Argentinian collaboration.

Author contribution statement

We arrange the manuscript contributions into three main categories, concerning the analytical studies and physical interpretation, numerical implementations and the writing of the current manuscript. The order reflects the relative additions by each author to the given item.

- analytical studies/physical interpretation: Ambrosio, Ancarani, Gómez, Gasaneo.
- numerical implementations: Ambrosio, Gómez, Mitnik, Gaggioli.
- writing process: Ancarani, Ambrosio, Gómez, Gaggioli.

References

1. D. Fischer, R. Moshammer, A. Dorn, J.R. Crespo López-Urrutia, B. Feuerstein, C. Höhr, C.D. Schröter, S. Hagmann, H. Kollmus, R. Mann, B. Bapat, J. Ullrich, Phys. Rev. Lett. **90**, 243201 (2003)
2. M.B. Shah, H.B. Gilbody, J. Phys. B: At. Mol. Phys. **18**, 899 (1985)
3. L.H. Andersen, P. Hvelplund, H. Knudsen, S.P. Møller, K. Elsener, K.G. Rensfelt, E. Uggerhøj, Phys. Rev. Lett. **57**, 2147 (1986)
4. L.H. Andersen, P. Hvelplund, H. Knudsen, S.P. Moller, J.O.P. Pedersen, S. Tang-Petersen, E. Uggerho/j, K. Elsener, E. Morenzoni, Phys. Rev. A **41**, 6536 (1990)
5. M. Schulz, R. Moshammer, W. Schmitt, H. Kollmus, B. Feuerstein, R. Mann, S. Hagmann, J. Ullrich, Phys. Rev. Lett. **84**, 863 (2000)
6. D. Fischer, M. Schulz, R. Moshammer, J. Ullrich, J. Phys. B: At. Mol. Opt. Phys. **37**, 1103 (2004)
7. M. Schulz, D. Fischer, R. Moshammer, J. Ullrich, J. Phys. B: At. Mol. Opt. Phys. **38**, 1363 (2005)
8. M. Schulz, D. Fischer, T. Ferger, R. Moshammer, J. Ullrich, J. Phys. B: At. Mol. Opt. Phys. **40**, 3091 (2007)
9. D. Fischer, M. Schulz, K. Schneider, M.F. Ciappina, T. Kirchner, A. Kelkar, S. Hagman, M. Grieser, K.-U. Kühnel, R. Moshammer, J. Ullrich, Phys. Rev. A **80**, 062703 (2009)
10. S.D. López, C.R. Garibotti, S. Otranto, Phys. Rev. A **83**, 062702 (2011)
11. S.D. López, S. Otranto, C.R. Garibotti, Phys. Rev. A **87**, 022705 (2013)
12. M.J. Ambrosio, D.M. Mitnik, L.U. Ancarani, G. Gasaneo, E.L. Gaggioli, Phys. Rev. A **92**, 042704 (2015)
13. M. Foster, J. Colgan, M.S. Pindzola, J. Phys. B: At. Mol. Opt. Phys. **41**, 111002 (2008)
14. M.F. Ciappina, M. Schulz, T. Kirchner, D. Fischer, R. Moshammer, J. Ullrich, Phys. Rev. A **77**, 062706 (2008)
15. X. Guan, K. Bartschat, Phys. Rev. Lett. **103**, 213201 (2009)
16. M. Schulz, M.F. Ciappina, T. Kirchner, D. Fischer, R. Moshammer, J. Ullrich, Phys. Rev. A **79**, 042708 (2009)
17. L. Gulyás, A. Igarashi, T. Kirchner, Phys. Rev. A **86**, 024701 (2012)
18. G. Gasaneo, D.M. Mitnik, J.M. Randazzo, L.U. Ancarani, F.D. Colavecchia, Phys. Rev. A **87**, 042707 (2013)
19. M.J. Ambrosio, F.D. Colavecchia, G. Gasaneo, D.M. Mitnik, L.U. Ancarani, J. Phys. B: At. Mol. Opt. Phys. **48**, 055204 (2015)
20. A. Dorn, A.S. Kheifets, C. Schröter, B. Najjari, C. Höhr, R. Moshammer, J. Ullrich, Phys. Rev. Lett. **86**, 3755 (2001)
21. M.J. Ambrosio, D.M. Mitnik, A. Dorn, L.U. Ancarani, G. Gasaneo, Phys. Rev. A **93**, 032705 (2016)
22. A.S. Kadyrov, A.M. Mukhamedzhanov, A.T. Stelbovics, I. Bray, F. Pirlepesov, Phys. Rev. A **68**, 022703 (2003)
23. M.J. Ambrosio, F.D. Colavecchia, D.M. Mitnik, G. Gasaneo, Phys. Rev. A **91**, 012704 (2015)
24. G. Gasaneo, L.U. Ancarani, D.M. Mitnik, J.M. Randazzo, A.L. Frapiccini, F.D. Colavecchia, Adv. Quantum Chem. **67**, 153 (2013)
25. J.M. Randazzo, L.U. Ancarani, G. Gasaneo, A.L. Frapiccini, F.D. Colavecchia, Phys. Rev. A **81**, 042520 (2010)
26. J.M. Randazzo, A.L. Frapiccini, F.D. Colavecchia, G. Gasaneo, Phys. Rev. A **79**, 022507 (2009)
27. J.M. Randazzo, A.L. Frapiccini, F.D. Colavecchia, G. Gasaneo, Int. J. Quantum Chem. **109**, 125 (2009)
28. J.M. Randazzo, D.M. Mitnik, G. Gasaneo, L.U. Ancarani, F. Colavecchia, Eur. J. Phys. D **69**, 189 (2015)
29. D. Fischer, private communication
30. S.D. López, C.R. Garibotti, S. Otranto, Nucl. Instrum. Meth. B **283**, 63 (2012)
31. A.S. Kheifets, I. Bray, J. Berakdar, C. Dal Cappello, J. Phys. B **35**, L15 (2002)
32. A. Dorn, A. Kheifets, C. Schröter, B. Najjari, C. Höhr, R. Moshammer, J. Ullrich, Phys. Rev. A **65**, 032709 (2002)
33. A.S. Kheifets, Phys. Rev. A **69**, 032712 (2004)